ACS OMEGA

http://pubs.acs.org/journal/acsodf Article

Revisiting the Mechanism of Electric Field Sensing in Graphene Devices

Afsal Kareekunnan,[‖] Tatsufumi Agari,[‖] Ahmed M. M. Hammam, Takeshi Kudo, Takeshi Maruyama, Hiroshi Mizuta, and Manoharan Muruganathan*

Cite This: *ACS Omega* 2021, 6, 34086−34091

Read Online

ACCESS | Metrics & More | Article Recommendations

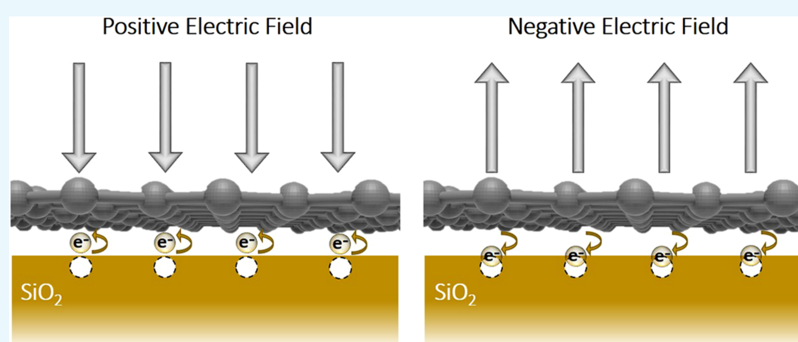

ABSTRACT: Electric field sensing has various real-life applications, such as early prediction of lightning. In this study, we effectively used graphene as an electric field sensor that can detect both positive and negative electric fields. The response of the sensor is recorded as the change in drain current under the application of an electric field. In addition, by systematic analysis, we established the mechanism of the graphene electric field sensor, and it is found to be different from the previously proposed one. The mechanism relies on the transfer of electrons between graphene and the traps at the SiO_2/graphene interface. While the direction of charge transfer depends on the polarity of the applied electric field, the amount of charge transferred depends on the magnitude of the electric field. Such a charge transfer changes the carrier concentration in the graphene channel, which is reflected as the change in drain current.

■ INTRODUCTION

Electric field sensing has important applications in our day-to-day lives, such as prediction of lightning and detection of supersonic aircraft. Conventional electric field sensors consist of electric field mills[1,2] and MEMS electric field sensors.[3−7] While field mills are massive in size and have rotating parts that are prone to failure, MEMS-based sensors require complex fabrication processes. In addition, these sensors require external amplification of the signal to achieve high sensitivity. Thus, it is vital to have an electric field sensor that has a mechanism different from that of the conventional electric field sensors while maintaining high sensitivity. To this end, graphene and analogous two-dimensional nanomaterials, which have proven to be excellent candidates for various sensing applications, are of paramount importance.[8] The unique band structure of graphene, where a slight change in the charge density is reflected in the electrical characteristics, makes it an ideal platform for sensing-based applications.[9−12] The carrier density in graphene is highly sensitive to external perturbations such as light, magnetic field, strain, adsorption of charged molecules, presence of charge traps in the dielectric layer, etc.[13−19] In this study, we explore the use of graphene as an electric field sensor and confirm the sensing mechanism.

Although graphene is widely used for various sensing applications, the potential of graphene as an electric field sensor and thereby extending the scope to the early prediction of lightning is lacking.[13] Wang et al. have studied graphene for electric field sensing and could detect electric fields as low as 200 V/m.[20] While they attribute the sensing mechanism to the drift of carriers to the traps at the Si/SiO_2 interface and the resultant capacitive coupling-induced drain current change in graphene, our study reveals that rather than the traps at the Si/SiO_2 interface, the traps at the SiO_2/graphene interface play the major role in electric field sensing in graphene. These surface traps, which originate from the defects and impurities, are positively

Received: October 5, 2021
Accepted: November 24, 2021
Published: December 3, 2021

ACS Publications © 2021 The Authors. Published by American Chemical Society

charged Coulomb-attractive centers that trap and detrap electrons to and from graphene under the application of an electric field.[21] Thus, in this study, by systematically analyzing various possibilities, we confirm the sensing mechanism in graphene electric field sensors.

■ RESULTS AND DISCUSSION

Figure 1a shows the schematic representation of our graphene device. The fabrication process is as follows. Graphene is exfoliated on a lightly doped silicon substrate (40−60 Ω·cm) with a SiO_2 of thickness 90 nm. Single-layer graphene is identified using optical contrast and later confirmed by Raman spectroscopy. The metal contacts are fabricated using electron-beam lithography, followed by the deposition of chromium and gold (5/60 nm) using electron beam evaporation. The hBN-encapsulated device and the device with hBN as a top dielectric is fabricated using the hot pick-up technique.[22,23] Figure 1b shows the schematic representation of the electric field measurement setup. The wire-bonded device is placed between two parallel disks separated by a working distance (WD) of 3 cm. Positive as well as negative external sources with a range of 10 V to 5 kV are used to apply the desired potential at the top plate. The bottom plate is connected to the ground. Figure 1c,d shows the response of the graphene device for positive and negative electric fields, respectively. The magnitude of the applied electric field is 16.67 kV/m. The measurement procedure is as follows. Initially, an electric field of the desired magnitude (16.67 kV/m in this case) is applied across the parallel disks. Next, the drain current measurement as a function of time is initiated. A constant source−drain voltage of 100 mV is applied across the terminals. While the drain current is being measured, the electric field across the plate is turned off. The dotted lines represent the time at which the electric field is turned off. As seen in the figure, the device responds differently to positive and negative electric fields. Under a positive electric field, the drain current is reduced, whereas under a negative electric field, the drain current is increased. The mechanism behind such behavior will be explained later. It can also be noted that while the drain current decreases(increases) for the positive(negative) electric field, the amount of change is similar in both cases (around 2.2 μA).

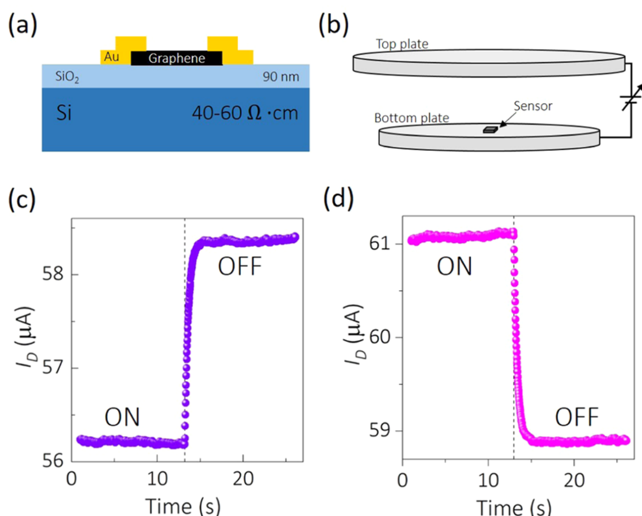

Figure 1. (a) Schematic diagram showing the graphene device structure. (b) Schematic representation of the graphene electric field measurement setup, which consists of two parallel metallic disks across which a static voltage is applied. The graphene sensor is placed between them as shown in the figure. Response of the graphene electric field sensor for (c) positive and (d) negative electric fields. In both cases, an electric field of magnitude 16.67 kV/m is applied across the parallel disks.

One of the important aspects of electric field sensing is the ability to sense the smallest electric field possible. As one would expect, the difference in the drain current in the presence and absence of the field will change with the strength of the applied electric field. The higher(lower) the electric field, the larger(smaller) the difference in the drain current. Thus, we define the electric field sensitivity (S_{EF}) of the sensor as the percentage change in the drain current.

$$S_{EF} = \frac{|I_{ON} - I_{OFF}|}{I_{OFF}} \times 100$$

where I_{ON} and I_{OFF} are the drain current in the presence and absence of the electric field, respectively. Figure 2a shows the sensitivity calculated as a function of the electric field applied across the parallel disks for both positive as well as negative

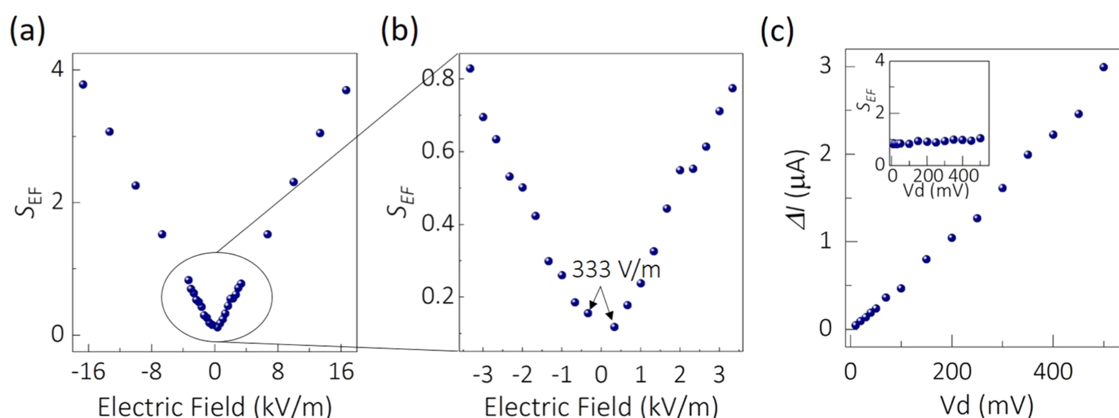

Figure 2. (a) Sensitivity as a function of the electric field applied across the parallel disks for both positive and negative polarities. (b) Zoomed-in image of the circled area in (a) showing the sensitivity for small electric fields. The magnitude of the lowest electric field detected (333 V/m) is highlighted for both positive and negative electric fields. (c) Difference in the drain current in the presence and absence of electric field ($\Delta I = I_{OFF} - I_{ON}$) as a function of the source−drain voltage applied across the terminals of the graphene device (electric field applied: 3.3 kV/m). Although the ΔI increases linearly with the source−drain voltage, the sensitivity remains nearly the same (inset).

https://doi.org/10.1021/acsomega.1c05530
ACS Omega 2021, 6, 34086−34091

cases. It can be seen that the sensitivity has a linear relationship with the field strength. Figure 2b is the magnified version of the area highlighted in Figure 2a showing the sensitivity for lower electric fields. The lowest electric field detected by the graphene sensor is 333 V/m, which is comparable to the one detected by the previous study (200 V/m).[20]

In all of the above measurements, the source−drain voltage applied across the graphene terminals was kept at 100 mV. Thus, we studied the effect of the source−drain voltage on various aspects of the electric field sensing in graphene. Figure 2c shows the difference in drain current without and with the application of electric field ($\Delta I = I_{OFF} - I_{ON}$) as a function of the source−drain voltage. The measurements are performed under an electric field of 3.3 kV/m applied across the parallel disks. Although the change in drain current shows a linear relationship with the source−drain bias, the electric field sensitivity remains constant (Figure 2c inset), implying that the increase in source−drain bias does not necessarily improve the sensitivity in the graphene electric field sensor.

As it became evident that graphene can be an excellent electric field sensor, it is vital to understand the mechanism of the sensing to further the study, especially to enhance the sensitivity. The mechanism proposed by Wang et al.,[20] has the following key elements: (i) graphene shields the electric field as it is grounded at one of its source−drain electrodes. (ii) Thus, the field around the graphene drifts carriers in the bulk of Si to the traps at the Si/SiO_2 interface. The trapped charges dope the graphene with opposite polarity through capacitive coupling, which varies the drain current. However, our experimental observations suggest that rather than the traps at the Si/SiO_2 interface, the traps at the SiO_2/graphene interface could be playing an important role in the mechanism of electric field sensing in graphene. Thus, we conducted a systematic analysis to validate this argument as described below.

(i) To check whether the external electric field must pass through graphene, we fabricated a graphene device where the graphene is completely covered with gold with a hexagonal boron nitride (hBN) dielectric layer between them (Figure 3a). The gold on top of graphene will completely block the electric field from reaching the graphene. Figure 3b shows the electric field response diagram of the gold-covered graphene device. A high electric field of 33.3 kV/m is applied across the parallel disks. No apparent difference in the drain current is observed with the application of the electric field. This confirms that to see the electric field sensing response in graphene in terms of the change in drain current, the electric field has to reach the graphene layer.

(ii) The next key aspect is to understand the role of the interfacial traps in the sensing mechanism of the graphene electric field sensor. To this end, we fabricated an hBN-encapsulated graphene device with a thick hBN at the bottom. It has been proven that the tunneling current from graphene through hBN decreases exponentially with the number of hBN layers.[24,25] Thus, we chose an hBN layer of thickness ∼40 nm at the bottom, expecting that it would prevent the transfer of charges from graphene to the traps at the interface. As per the mechanism proposed in the previous study,[20] the electric field hitting the substrate around the graphene drifts the carriers in silicon to the traps at the Si/SiO_2 interface. Thus, the presence of the thick hBN should not affect the electric field sensing. However, our measurements demonstrate that the encapsulated device with thick hBN underneath shows negligible sensitivity to the electric field. Figure 4a compares the electric field response of the encapsulated

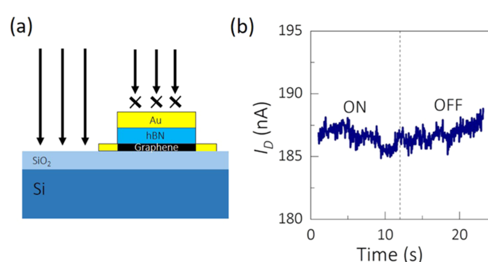

Figure 3. (a) Schematic diagram showing the graphene device completely covered with gold with a dielectric layer of hBN between them. The metal at the top acts as an electric field shield, blocking the field from reaching the graphene. (b) Electric field sensing response of the metal-covered graphene device. No noticeable change in the drain current is observed in the presence of the electric field, implying that the field has to reach graphene to induce a change in carrier concentration and thereby changing the drain current.

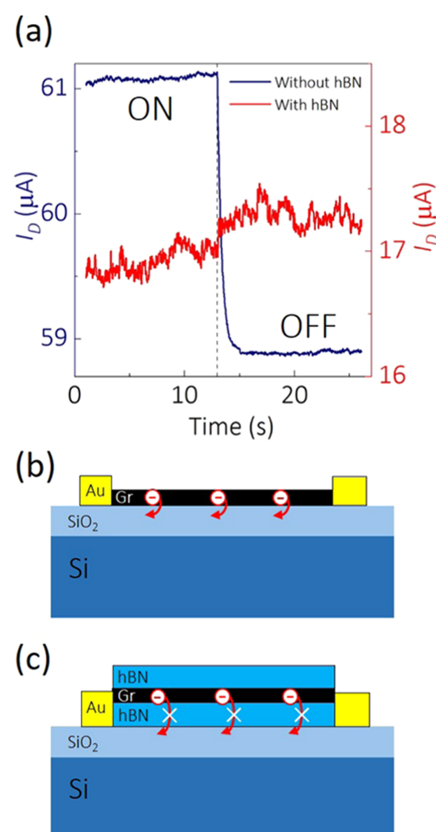

Figure 4. (a) Comparison of the electric field response of pristine graphene device and hBN-encapsulated graphene device with a thick hBN at the bottom. While the pristine graphene device shows a clear response in terms of the change in drain current in the presence and absence of the electric field, the hBN-encapsulated graphene device shows a negligible difference. Schematic diagrams illustrate (b) the transfer of electrons from graphene to the traps, resulting in a change in carrier concentration and drain current in pristine graphene, whereas (c) the thick hBN at the bottom in the case of encapsulated device prevents the transfer of charges from graphene to the traps, resulting in a negligible difference in drain current.

https://doi.org/10.1021/acsomega.1c05530
ACS Omega 2021, 6, 34086−34091

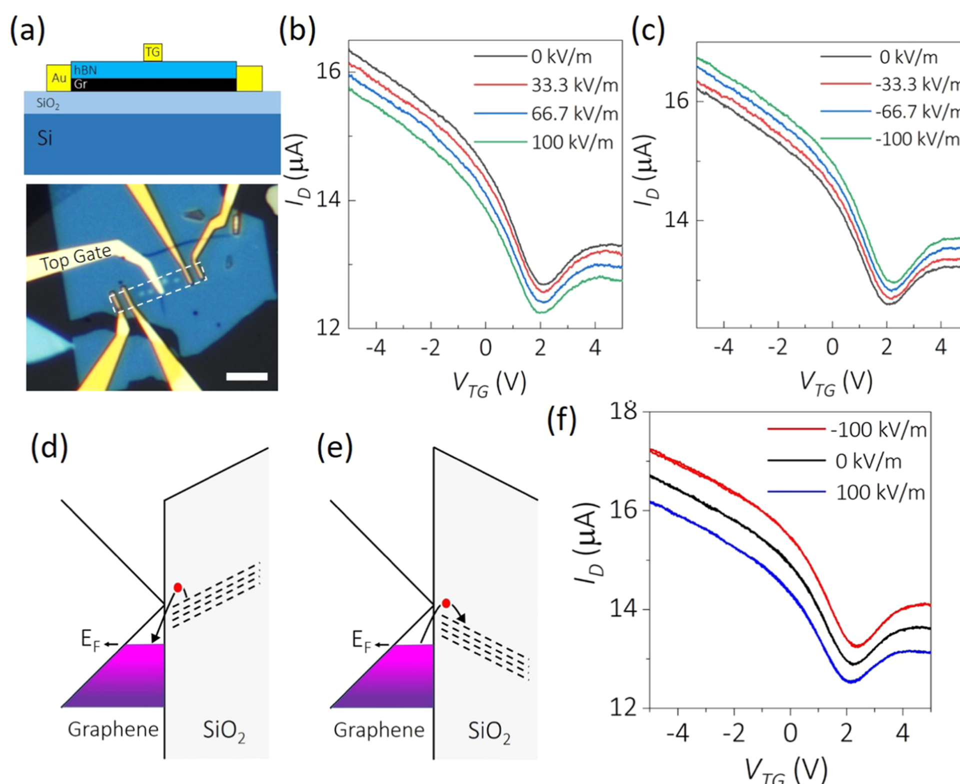

Figure 5. (a) Schematic diagram and optical micrograph of the top-gated device. The white dotted lines outline the graphene region. The scale bar is 10 μm. Top-gate characteristics of the graphene device under (b) positive and (c) negative electric fields of various strengths. Schematic diagram showing (d) the release of electrons from the traps to the graphene under a positive electric field and (e) the transfer of electrons from graphene to the interface traps under a negative electric field. (f) Dual sweep top-gate characteristics of the graphene device in the absence of an electric field as well as for both positive and negative electric fields.

device with that of the pristine graphene device. Both measurements are performed under a negative electric field of magnitude 16.67 kV/m. A source−drain voltage of 100 mV is applied across the graphene terminals. It can be seen that while the pristine graphene device shows a clear change in the drain current in the presence of an electric field, the hBN-encapsulated device shows no noticeable change. This indicates that for the pristine graphene device, the change in drain current in the presence of an electric field comes from the transfer of charges from the graphene to the traps at the SiO_2/graphene interface and the resultant change in the carrier concentration in graphene, as shown schematically in Figure 4b. As for the encapsulated device, the thick hBN at the bottom prevents the transfer of charges from the graphene to the traps at the interface (Figure 4c). This unequivocally proves the role of traps at the SiO_2/graphene interface in the sensing mechanism of the graphene electric field sensor.

Now that we have established the basic mechanism of electric field sensing in graphene devices, we studied the gate characteristics of the device to gain further understanding of the mechanism. Thus, we fabricated a top-gated device with hBN as the dielectric between graphene and the top electrode (Figure 5a). A narrow top electrode was fabricated so that the major area of the graphene is exposed to the field (the dotted white line outline the graphene region). Figure 5b,c shows the top-gate characteristics of the device for different positive and negative electric fields, respectively. The source−drain voltage applied in all of the measurements is 100 mV. The asymmetry in the electron and hole branches of drain current is the result of scattering from inhomogeneous charged impurities in graphene.[17,26,27] The gate characteristics for the positive electric field show a consistent decrease in the drain current with the increase in the field strength (Figure 5b). Further, the charge neutrality point (CNP) shifts toward the negative gate voltage, indicating n-doping of the graphene channel. The above observations can be explained in the light of charge transfer between graphene and the SiO_2/graphene interface as follows. Graphene, being p-doped, has the Fermi level in the valence band. Under a positive electric field, the electrons from the traps are released into the graphene (Figure 5d), resulting in n-doping of the graphene and the shift of CNP toward negative gate voltage. Moreover, the electrons injected into the graphene shift the Fermi level up, reducing the density of states and hence the drain current. This is consistent with the decrease in the drain current for the positive electric field in the response diagram of the sensor (Figure 1c). As for the negative electric field, the top-gate characteristics show an opposite trend to that of the positive electric field as anticipated (Figure 5c). The charge neutrality point shifts toward higher positive gate voltages and the drain current increases with the increase in the field strength. This implies that under a negative electric field, the electrons from graphene are pushed to the traps at the interface (Figure 5e). This leads to further p-doping of graphene, seen as the right shift of CNP. Additionally, the downward shift of the Fermi level as a result of increased p-doping increases the density of states, which in turn increases the drain current. This explains the response diagram for the negative electric field where an increase in drain current is observed in the presence of the field (Figure

https://doi.org/10.1021/acsomega.1c05530
ACS Omega 2021, 6, 34086−34091

1d). The purpose of using a top gate with hBN as the dielectric is to eliminate the effect of gate voltage sweeping on the trapping and detrapping of the charges so that the sole effect of the electric field on these processes could be understood. It has already been reported that the gate voltage sweep can introduce hysteresis in the gate characteristics due to the transfer of charges between graphene and the traps at the dielectric interface.[28−35] However, hBN, which is a highly crystalline two-dimensional material, has negligible defects. Figure 5f shows the dual sweep top-gate characteristics of the device in the absence of the electric field as well as for both positive and negative electric fields. No change in the drain current and CNP is observed between the forward and backward sweep in any of the cases. This suggests that the gate voltage sweep does not have any effect on the trapping and detrapping processes. Furthermore, observing an apparent response to both positive and negative electric fields with the top-gated device where the hBN covers the graphene completely confirms that the top hBN did not impact the observed results for the gold-covered device (Figure 3) and the device with thick hBN underneath (Figure 4a,c).

CONCLUSIONS

In conclusion, we have successfully used graphene as an electric field sensor that can detect both positive and negative electric fields. The lowest electric field detected by the graphene sensor is 333 V/m. Also, by systematic analysis, we confirmed the mechanism of electric field sensing, which is attributed to the transfer of electrons between graphene and the traps at the SiO_2/graphene interface. The direction of electron transfer depends on the polarity of the applied electric field. Under a positive electric field, the electrons are transferred from traps to the graphene, while under a negative electric field, electrons are transferred from graphene to the traps.

AUTHOR INFORMATION

Corresponding Author

Manoharan Muruganathan − *Japan Advanced Institute of Science and Technology, Nomi 923-1292, Japan;* orcid.org/0000-0001-5421-5160; Email: mano@jaist.ac.jp

Authors

Afsal Kareekunnan − *Japan Advanced Institute of Science and Technology, Nomi 923-1292, Japan*

Tatsufumi Agari − *Japan Advanced Institute of Science and Technology, Nomi 923-1292, Japan*

Ahmed M. M. Hammam − *Physics Department, Faculty of Science, Minia University, Minia 61519, Egypt*

Takeshi Kudo − *Otowa Electric Co., Ltd., Hyogo 661-0976, Japan*

Takeshi Maruyama − *Otowa Electric Co., Ltd., Hyogo 661-0976, Japan*

Hiroshi Mizuta − *Japan Advanced Institute of Science and Technology, Nomi 923-1292, Japan*

Complete contact information is available at: https://pubs.acs.org/10.1021/acsomega.1c05530

Author Contributions

[‖]A.K. and T.A. contributed equally to this work.

Notes

The authors declare no competing financial interest.

ACKNOWLEDGMENTS

The authors acknowledge the support from Center of Innovation (CoI) JPMJCE1309, JST Adaptable and Seamless Technology Transfer Program through Target-driven R&D (A-STEP) Grant Number JPMJTM20DS and Otowa Electric Co., Ltd.

REFERENCES

(1) Kaplan, B.-Z.; Suissa, U. Duality of the electric covering fieldmill and the fluxgate magnetometer. *IEEE Trans. Magn.* **1998**, *34*, 2306−2315.
(2) Taylor, D. Measuring techniques for electrostatics. *J. Electrost.* **2001**, *51*−*52*, 502−508.
(3) Horenstein, M. N.; Stone, P. R. A micro-aperture electrostatic field mill based on MEMS technology. *J. Electrost.* **2001**, *51*−*52*, 515−521.
(4) Peng, C.; Chen, X.; Ye, C.; Tao, H.; Cui, G.; Bai, Q.; Chen, S.; Xia, S. Design and testing of a micromechanical resonant electrostatic field sensor. *J. Micromech. Microeng.* **2006**, *16*, 914−919.
(5) Bahreyni, B.; Wijeweera, G.; Shafai, C.; Rajapakse, A. Analysis and Design of a Micromachined Electric-Field Sensor. *J. Microelectromech. Syst.* **2008**, *17*, 31−36.
(6) Kobayashi, T.; Oyama, S.; Takahashi, M.; Maeda, R.; Itoh, T. Microelectromechanical Systems-Based Electrostatic Field Sensor Using Pb(Zr,Ti)O_3 Thin Films. *Jpn. J. Appl. Phys.* **2008**, *47*, 7533−7536.
(7) Yang, P.; Peng, C.; Fang, D.; Wen, X.; Xia, S. Design, fabrication and application of an SOI-based resonant electric field microsensor with coplanar comb-shaped electrodes. *J. Micromech. Microeng.* **2013**, *23*, No. 055002.
(8) Liu, B.; Zhou, K. Recent progress on graphene-analogous 2D nanomaterials: Properties, modeling and applications. *Prog. Mater. Sci.* **2019**, *100*, 99−169.
(9) Novoselov, K. S.; Geim, A. K.; Morozov, S. V.; Jiang, D.; Zhang, Y.; Dubonos, S. V.; Grigorieva, I. V.; Firsov, A. A. Electric Field Effect in Atomically Thin Carbon Films. *Science* **2004**, *306*, 666−669.
(10) Novoselov, K. S.; Jiang, D.; Schedin, F.; Booth, T. J.; Khotkevich, V. V.; Morozov, S. V.; Geim, A. K. Two-dimensional atomic crystals. *Proc. Natl. Acad. Sci. U.S.A.* **2005**, *102*, 10451−10453.
(11) Novoselov, K. S.; Geim, A. K.; Morozov, S. V.; Jiang, D.; Katsnelson, M. I.; Grigorieva, I. V.; Dubonos, S. V.; Firsov, A. A. Two-dimensional gas of massless Dirac fermions in graphene. *Nature* **2005**, *438*, 197−200.
(12) Geim, A. K.; Novoselov, K. S. The rise of graphene. *Nat. Mater.* **2007**, *6*, 183−191.
(13) Hill, E. W.; Vijayaragahvan, A.; Novoselov, K. Graphene Sensors. *IEEE Sens. J.* **2011**, *11*, 3161−3170.
(14) Novoselov, K. S.; Falko, V. I.; Colombo, L.; Gellert, P. R.; Schwab, M. G.; Kim, K. A roadmap for graphene. *Nature* **2012**, *490*, 192−200.
(15) Kostarelos, K.; Novoselov, K. S. Graphene devices for life. *Nat. Nanotechnol.* **2014**, *9*, 744−745.
(16) Yu, X.; Cheng, H.; Zhang, M.; Zhao, Y.; Qu, L.; Shi, G. Graphene-based smart materials. *Nat. Rev. Mater.* **2017**, *2*, No. 17046.
(17) Adam, S.; Hwang, E. H.; Galitski, V. M.; das Sarma, S. A self-consistent theory for graphene transport. *Proc. Natl. Acad. Sci. U.S.A.* **2007**, *104*, 18392−18397.
(18) Tan, Y.-W.; Zhang, Y.; Bolotin, K.; Zhao, Y.; Adam, S.; Hwang, E. H.; das Sarma, S.; Stormer, H. L.; Kim, P. Measurement of Scattering Rate and Minimum Conductivity in Graphene. *Phys. Rev. Lett.* **2007**, *99*, No. 246803.
(19) Chen, J.-H.; Jang, C.; Adam, S.; Fuhrer, M. S.; Williams, E. D.; Ishigami, M. Charged-impurity scattering in graphene. *Nat. Phys.* **2008**, *4*, 377−381.
(20) Wang, W.; Du, R.; Zafar, A.; He, L.; Zhao, W.; Chen, Y.; Lu, J.; Ni, Z. High-Performance Graphene-Based Electrostatic Field Sensor. *IEEE Electron Device Lett.* **2017**, *38*, 1136−1138.
(21) Kim, Y. D.; Bae, M.-H.; Seo, J.-T.; Kim, Y. S.; Kim, H.; Lee, J. H.; Ahn, J. R.; Lee, S. W.; Chun, S.-H.; Park, Y. D. Focused-Laser-Enabled

p−n Junctions in Graphene Field-Effect Transistors. *ACS Nano* **2013**, *7*, 5850−5857.
(22) Wang, L.; Meric, I.; Huang, P. Y.; Gao, Q.; Gao, Y.; Tran, H.; Taniguchi, T.; Watanabe, K.; Campos, L. M.; Muller, D. A.; Guo, J.; Kim, P.; Hone, J.; Shepard, K. L.; Dean, C. R. One-Dimensional Electrical Contact to a Two-Dimensional Material. *Science* **2013**, *342*, 614−617.
(23) Pizzocchero, F.; Gammelgaard, L.; Jessen, B. S.; Caridad, J. M.; Wang, L.; Hone, J.; Bøggild, P.; Booth, T. J. The hot pick-up technique for batch assembly of van der Waals heterostructures. *Nat. Commun.* **2016**, *7*, No. 11894.
(24) Britnell, L.; Gorbachev, R. V.; Jalil, R.; Belle, B. D.; Schedin, F.; Katsnelson, M. I.; Eaves, L.; Morozov, S. V.; Mayorov, A. S.; Peres, N. M. R.; Castro Neto, A. H.; Leist, J.; Geim, A. K.; Ponomarenko, L. A.; Novoselov, K. S. Electron Tunneling through Ultrathin Boron Nitride Crystalline Barriers. *Nano Lett.* **2012**, *12*, 1707−1710.
(25) Britnell, L.; Gorbachev, R. V.; Jalil, R.; Belle, B. D.; Schedin, F.; Mishchenko, A.; Georgiou, T.; Katsnelson, M. I.; Eaves, L.; Morozov, S. V.; Peres, N. M. R.; Leist, J.; Geim, A. K.; Novoselov, K. S.; Ponomarenko, L. A. Field-Effect Tunneling Transistor Based on Vertical Graphene Heterostructures. *Science* **2012**, *335*, 947−950.
(26) Hwang, E. H.; Adam, S.; Sarma, S. D. Carrier Transport in Two-Dimensional Graphene Layers. *Phys. Rev. Lett.* **2007**, *98*, No. 186806.
(27) Chen, J.-H.; Jang, C.; Adam, S.; Fuhrer, M. S.; Williams, E. D.; Ishigami, M. Charged-impurity scattering in graphene. *Nat. Phys.* **2008**, *4*, 377−381.
(28) Wang, H.; Wu, Y.; Cong, C.; Shang, J.; Yu, T. Hysteresis of Electronic Transport in Graphene Transistors. *ACS Nano* **2010**, *4*, 7221−7228.
(29) Liao, Z.-M.; Han, B.-H.; Zhou, Y.-B.; Yu, D.-P. Hysteresis reversion in graphene field-effect transistors. *J. Chem. Phys.* **2010**, *133*, No. 044703.
(30) Li, H.; Zhang, Q.; Liu, C.; Xu, S.; Gao, P. Ambipolar to Unipolar Conversion in Graphene Field-Effect Transistors. *ACS Nano* **2011**, *5*, 3198−3203.
(31) Imam, S. A.; Deshpande, T.; Guermoune, A.; Siaj, M.; Szkopek, T. Charge transfer hysteresis in graphene dual-dielectric memory cell structures. *Appl. Phys. Lett.* **2011**, *99*, No. 082109.
(32) Kim, S. M.; Song, E. B.; Lee, S.; Zhu, J.; Seo, D. H.; Mecklenburg, M.; Seo, S.; Wang, K. L. Transparent and Flexible Graphene Charge-Trap Memory. *ACS Nano* **2012**, *6*, 7879−7884.
(33) Lee, S.; Song, E. B.; Kim, S.; Seo, D. H.; Seo, S.; Kang, T. W.; Wang, K. L. Impact of gate work-function on memory characteristics in $Al_2O_3/HfO_x/Al_2O_3$/graphene charge-trap memory devices. *Appl. Phys. Lett.* **2012**, *100*, No. 023109.
(34) Lee, S.; Song, E. B.; Min Kim, S.; Lee, Y.; Seo, D. H.; Seo, S.; Wang, K. L. Reduced electron back-injection in $Al_2O_3/AlO_x/Al_2O_3$/graphene charge-trap memory devices. *Appl. Phys. Lett.* **2012**, *101*, No. 243109.
(35) Peng, S.; Jin, Z.; Yao, Y.; Huang, X.; Zhang, D.; Niu, J.; Shi, J.; Zhang, Y.; Yu, G. Controllable p-to-n Type Conductance Transition in Top-Gated Graphene Field Effect Transistor by Interface Trap Engineering. *Adv. Electron. Mater.* **2020**, *6*, No. 2000496.

https://doi.org/10.1021/acsomega.1c05530
ACS Omega 2021, 6, 34086−34091